dence, T^* increasing with decreasing T_c, is the expected one for such a pseudogap. But the values of T^* are different for the two samples. Other processes, such as localization by defects, most likely are in play, because in underdoped cuprates the value of the characteristic energy T^* does not change substantially between different samples (*21*).

References and Notes

1. W. L. McMillan, *Phys. Rev.* **167**, 331 (1968).
2. V. L. Ginzburg, D. A. Kirzhnits, Eds., *High Temperature Superconductivity* (Consultants Bureau, New York, 1982).
3. P. W. Anderson, *Science* **288**, 480 (2000).
4. J. H. Schön, Ch. Kloc, B. Batlogg, *Nature* **408**, 549 (2000).
5. J. Akimitsu, paper presented at the Symposium on Transition Metal Oxides, Sendai, Japan, 10 January 2001.
6. J. Kortus, I. I. Mazin , K. D. Belashchenko, V. P. Antropov, L. L. Boyer, e-Print available at http://arXiv.org/abs/cond-mat/0101446.
7. S. L. Bud'ko *et al.*, *Phys. Rev. Lett.* **86**, 1877 (2001) (e-Print available at http://arXiv.org/abs/cond-mat/0101463).
8. J. E. Hirsch, e-Print available at http://arXiv.org/abs/cond-mat/0102115.
9. S. Sanfilippo *et al.*, *Phys. Rev. B* **61**, R3800 (2000).
10. P. Bordet *et al.*, *Phys. Rev. B* **62**, 11392 (2000).
11. C. W. Chu *et al.*, *Nature* **365**, 323 (1993).
12. M. Núñez-Regueiro, J.-L. Tholence, E. V. Antipov, J.-J. Capponi, M. Marezio, *Science* **262**, 97 (1993).
13. L. Gao *et al.*, *Phys. Rev. B* **50**, 4260 (1994).
14. P. M. Horn, C. Guidotti, *Phys. Rev. B* **16**, 491 (1977).
15. B. Abeles, P. Sheng, M. D. Coutts, Y. Arie, *Adv. Phys.* **24**, 407 (1975).
16. R. J. Cava *et al.*, *Nature* **367**, 146 (1994).
17. M. Núñez-Regueiro *et al.*, *Physica C* **235–240**, 2093 (1994).
18. M. Núñez-Regueiro, C. Acha, in *Hg-Based High* T_c *Superconductors*, A. Narlikar, Ed., vol. 24 of *Studies of High Temperature Superconductors* (Nova Science, New York, 1997), pp. 203–240.
19. B. T. Matthias, in *Superconductivity of d- and f-Band Metals* (American Institute of Physics, New York, 1972), p. 367–376.
20. H. Takagi *et al.*, *Phys. Rev. Lett.* **69**, 2975 (1992).
21. D. K. Finnemore, J. E. Ostenson, S. L. Bud'ko, G. Lapertot, P. C. Canfield, e-Print available at http://arXiv.org/abs/cond-mat/0102114.

22. We acknowledge P. Monceau, B. Chakraverty, D. Núñez-Regueiro, C. Paulsen, and J.-L. Tholence for a critical reading of the manuscript and J. Ranninger and B. Batlogg for enlightening discussions. M.M. is a Consejo Nacional de Investigaciones Científicas y Técnicas (Argentina) doctoral fellow.

12 February 2001; accepted 22 February 2001
Published online 8 March 2001;
10.1126/science.1059775
Include this information when citing this paper.

Experimental Verification of a Negative Index of Refraction

R. A. Shelby, D. R. Smith, S. Schultz

We present experimental scattering data at microwave frequencies on a structured metamaterial that exhibits a frequency band where the effective index of refraction (*n*) is negative. The material consists of a two-dimensional array of repeated unit cells of copper strips and split ring resonators on interlocking strips of standard circuit board material. By measuring the scattering angle of the transmitted beam through a prism fabricated from this material, we determine the effective *n*, appropriate to Snell's law. These experiments directly confirm the predictions of Maxwell's equations that *n* is given by the negative square root of $\varepsilon \cdot \mu$ for the frequencies where both the permittivity (ε) and the permeability (μ) are negative. Configurations of geometrical optical designs are now possible that could not be realized by positive index materials.

Refraction is perhaps one of the most basic of electromagnetic phenomena, whereby when a beam of radiation is incident on an interface between two materials at an arbitrary angle, the direction of propagation of the transmitted beam is altered by an amount related to the indices of refraction of the two materials. Snell's law, arrived at by requiring that the phase of the incident and transmitted beams be the same everywhere at the interface, provides the quantitative relation between the incident and refractive angles (θ_1 and θ_2, measured from the refraction interface normal) and the indices of refraction of the media (n_1 and n_2), having the form $n_1 \sin(\theta_1) = n_2 \sin(\theta_2)$. A refracted ray is thus bent toward the normal (but never emerges on the same side of the normal as the incident ray) upon entering a naturally occurring material from air, as most materials have $n > 1$. Refraction forms the basis of lenses and imaging, as any finite section of material with an index differing from that of its environment will alter the direction of incoming rays that are not normal to the interface. Lenses can be designed to focus and steer radiation for a wide variety of applications and are of use over a large range of wavelengths (e.g., from radio to optical).

Although all known naturally occurring materials exhibit positive indices of refraction, the possibility of materials with negative refractive index has been explored theoretically (*1*) and the conclusion presented that such materials did not violate any fundamental physical laws. These materials were termed "left-handed" (LHM), and it was further shown that some of the most fundamental electromagnetic properties of an LHM would be opposite to that of ordinary "right-handed" materials (RHM), resulting in unusual and nonintuitive optics. A beam incident on an LHM from an RHM, for example, refracts to the same side of the normal as the incident ray. Furthermore, it was predicted that the rays from a point source impinging on a flat, parallel slab of LHM would be refocused to a point on the opposite side of the material. Recently, analysis of this situation produced the observation that such a planar slab, if of suitable index, can produce a focus with subwavelength resolution, beating the normal diffraction limit associated with positive refractive index optics (*2*).

The fabrication and measurement of structured metamaterials having a range of frequencies over which the refractive index was predicted to be negative for one direction of propagation were reported recently (*3*). An extension of this structure to two dimensions was subsequently introduced and predicted to exhibit an isotropic, negative index in two dimensions (*4*). These structures use split ring resonators to produce negative magnetic permeability over a particular frequency region (*5*) and wire elements to produce negative electric permittivity in an overlapping frequency region (*6*). When the permittivity, ε, and permeability, μ, of a material are simultaneously negative, one must choose the negative root of the index of refraction given by $n = \pm\sqrt{\varepsilon\mu/\varepsilon_0\mu_0}$ (ε_0 and μ_0 are the free-space permittivity and permeability, respectively) (*1*, *2*, *7*). Although the recent transmission experiments and simulations (*3*, *4*) on LHMs demonstrated the presence of a left-handed propagation band, the experiments presented here directly confirm that LHMs do indeed exhibit negative refraction.

The LHM sample used in the experiments presented here (Fig. 1) consists of a two-dimensionally periodic array of copper split ring resonators and wires, fabricated by a shadow mask/etching technique on 0.25-mm-thick G10 fiber glass circuit board material. After processing, the boards were cut and assembled into an interlocking unit, from which a prism-shaped section was cut for the beam-deflection experiments.

To determine the refractive index, we measured the deflection of a beam of microwave radiation as the beam passed through the prism-shaped sample. In this refraction experiment (Fig. 2), the prism-shaped samples were placed between the two circular

Department of Physics, University of California, San Diego, La Jolla, CA 92093–0350, USA.

aluminum plates. The top plate had a pivot in the center, about which an attached X-band microwave waveguide could be rotated to measure transmitted power at arbitrary refraction angles. The incident face of the prism was illuminated with a beam of microwaves whose electric field was polarized such that it was uniform and perpendicular to the metal plates and parallel to the wires shown in Fig. 1 (transverse magnetic polarization). Any refraction from the first surface would be caused by components of the incident beam containing angles of incidence away from the normal. To reduce the angular spread of the incident beam caused by diffraction from the source, we introduced the microwaves through a coaxial cable to waveguide adapter, 1 m distant from the sample. The waves were then guided by two flat sheets of aluminum whose spacing matched that of the circular plates (1.2 cm) and were laterally confined by sheets of absorber placed 9.3 cm apart.

After propagating through the sample, the microwave beam encounters the second surface of the prism, the refraction interface, and is refracted into a direction determined by Snell's law. To measure the exit angle, we rotated the waveguide/power meter assembly in 1.5° steps and recorded the transmitted power spectrum over the entire X-band range at each step, using an HP8756A scalar network analyzer. Experiments were performed with a prism-shaped LHM sample, as well as with a similarly shaped Teflon sample as a control. The normal to the LHM refraction surface was at an angle of 18.43° with respect to the normal of the incident surface. As can be seen in Fig. 3, at 10.5 GHz, the microwaves were refracted to positive angles as expected for the Teflon sample and to the opposite side (i.e., negative θ side) of the normal for the LHM sample. The Teflon data show refraction as would be predicted for $n_{\text{Teflon}} = 1.4 \pm 0.1$, whereas for the LHM, the measured exit angle of $\theta_{\text{air}} = -61°$ implies that $n_{\text{LHM}} = -2.7 \pm 0.1$.

Permeability, permittivity, and refractive index are bulk, effective medium properties. Although our metamaterial consists of discrete scattering elements, it may be approximated as an effective medium for wavelengths that are larger than the unit cell size. The LHM used in these experiments had a unit cell dimension of 5 mm, a factor of 6 smaller than the X-band (8 to 12 GHz) center wavelength of 3 cm. Previous studies have shown that frequency-dependent, effective material parameters describe well the transmission of normally incident plane waves through a planar slab of this material (*4*).

Although the structured LHM generally behaves analogously to a uniform material over the wavelengths studied, the finite unit cell size leads to an unavoidable corrugation of the refraction surface. We confirmed that this corrugation, in conjunction with reflection at the interface, introduces modulations into the observed angular transmission patterns, by observing the angular transmission from a Teflon sample that had been cut with a step pattern identical to that of the LHM sample (*8*). To present an average representation of the LHM data, we recorded transmitted power as a function of frequency and refraction angle for eight different sample positions. The nonequivalent positions were obtained by translating the LHM sample along the refraction surface in 2-mm steps. The eight sets of data were then averaged together and the results are shown in Fig. 3. The refraction peaks of all of the individual traces were positioned at similar negative angles.

Although negative refractive index does not violate any fundamental laws, causality places restrictions on the analytic form for the index as a function of frequency (*9*). Using Eqs. 1 and 2 as the generic forms of the frequency-dependent material parameters ε and μ (*4*–*6*), we can determine the expected frequency dependence of the index of refraction:

$$\frac{\mu(\omega)}{\mu_0} = 1 - \frac{\omega_{mp}^2 - \omega_{mo}^2}{\omega^2 - \omega_{mo}^2 + i\gamma\omega} \qquad (1)$$

where ω_{mo} is the magnetic resonance frequency, ω_{mp} is the "magnetic plasma frequency," $i = \sqrt{-1}$, and

$$\frac{\varepsilon(\omega)}{\varepsilon_0} = 1 - \frac{\omega_{ep}^2 - \omega_{eo}^2}{\omega^2 - \omega_{eo}^2 + i\gamma\omega} \qquad (2)$$

where ω_{eo} is the electronic resonance fre-

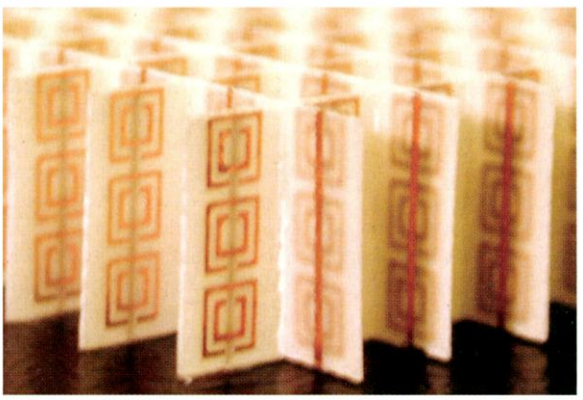

Fig. 1. Photograph of the left-handed metamaterial (LHM) sample. The LHM sample consists of square copper split ring resonators and copper wire strips on fiber glass circuit board material. The rings and wires are on opposite sides of the boards, and the boards have been cut and assembled into an interlocking lattice.

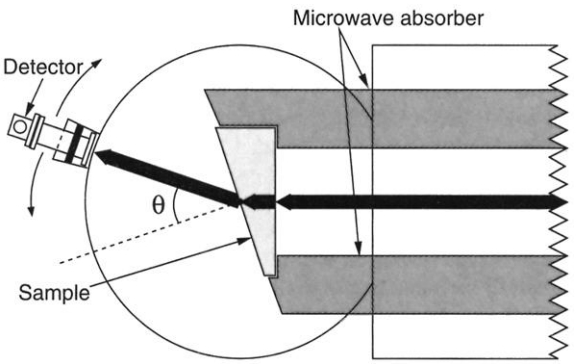

Fig. 2. Diagram of experimental setup. The sample and the microwave absorber were placed between top and bottom parallel, circular aluminum plates spaced 1.2 cm apart. The radius of the circular plates was 15 cm. The black arrows represent the microwave beam as would be refracted by a positive index sample. The detector was rotated around the circumference of the circle in 1.5° steps, and the transmitted power spectrum was measured as a function of angle, θ, from the interface normal. The detector was a waveguide to coaxial adapter attached to a standard X-band waveguide, whose opening was 2.3 cm in the plane of the circular plates. θ as shown is positive in this figure.

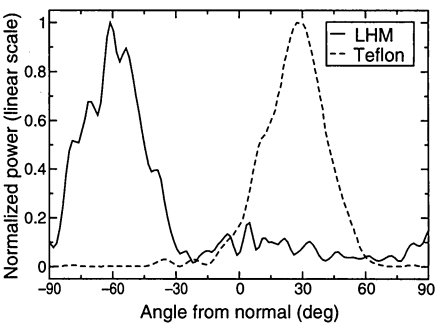

Fig. 3. Transmitted power at 10.5 GHz as a function of refraction angle for both a Teflon sample (dashed curve) and a LHM sample (solid curve). The two curves were normalized such that the magnitude of both peaks is unity. For the Teflon sample, the refracted power peak was measured to be 27°, corresponding to a positive index of refraction of 1.4 ± 0.1. For the LHM sample, the peak was at −61°, from which we deduce the index of refraction to be −2.7 ± 0.1. The beam width is set by diffraction at the exit of the incident channel and the angular sensitivity of the detector and is similar to the beam width that is measured without a sample in place.

quency and ω_{ep} is the electronic plasma frequency. When the wires do not maintain electrical continuity, as in these experiments, $\omega_{eo} > 0$.

In particular, over the band of frequencies that have been previously identified as the left-handed propagation region (ε and μ both negative, about 10.2 to 10.8 GHz), the index is expected to take very negative values on the low-frequency side of the left-handed band, passing through a value of zero on the high-frequency side. The measured index as a function of frequency for the LHM sample is presented (Fig. 4) and compared with theoretical predictions and similar data taken on the Teflon sample. Although the measured index for Teflon is basically flat across the X-band frequency range, the index of refraction for the LHM is negative over the left-handed frequency band and is highly dispersive, in a manner consistent with theoretical predictions (*7*). We used Eqs. 1 and 2 to calculate the theoretical curves using the following parameters: $f_{mp} = 10.95$ GHz, $f_{mo} = 10.05$ GHz, $f_{ep} = 12.8$ GHz, $f_{eo} = 10.3$ GHz, and $\gamma = 10$ MHz ($f = \omega/2\pi$).

We note two limitations on our experimental technique that prevent us from probing the effective index corresponding to the extremes of the left-handed frequency band. When the effective index approaches zero, the wavelength in the LHM becomes very large, presumably larger than the dimensions of the sample. Under these conditions, the sample is best characterized by a scattering cross section rather than interpreted with geometrical ray concepts. Thus, we are unable to unambiguously determine the index in the frequency region from about 10.8 to 12 GHz, which would correspond to an imaginary index rather than positive as measured. This limitation might be eased by the use of thicker and wider samples. Also, because we cut our refraction interface to be roughly 18.4° from normal incidence, when $|n| \gtrsim 3$, we expect the incident beam to undergo total internal reflection rather than refraction, possibly explaining the lack of observed index values below -3 and above $+3$.

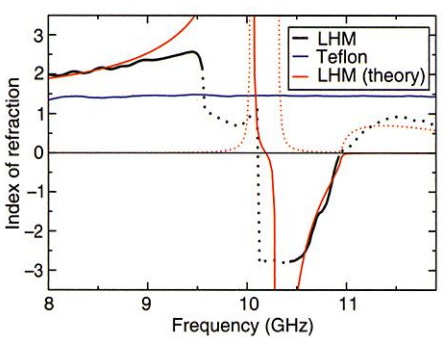

Fig. 4. Index of refraction versus frequency. The blue curve corresponds to data from the Teflon sample, and the black curve is for the LHM data. The dotted portions of the LHM curve indicate regions where the index is expected to be either outside our limit of detection ($|n| > 3$) or dominated by the imaginary component and therefore could not be reliably determined experimentally. The solid red curve is the real component, and the dotted red curve is the imaginary component of the theoretical expression for the refractive index as fit to the square root of the product of Eqs. 1 and 2 as described in the text.

An immediate question is whether the negative index-of-refraction property can be implemented at optical frequencies. It is unlikely that the inherent material properties of conductors will scale much past the infrared, rendering left-handed materials, such as those used here, ineffective. The phenomenon of negative refraction has recently been predicted by numerical simulations on dielectric, photonic crystals, at certain frequencies near negative group-velocity bands (*10*, *11*). Although the refracted beam may bend toward a negative angle in these systems, it is difficult to define an equivalent index of refraction with the same generality as we find in metamaterials, because these effects occur above the Bragg reflection frequency. Furthermore, surface waves at the interface between photonic crystals and other uniform media complicate the surface matching problem, making design considerations more difficult. Nevertheless, the use of photonic crystals as negative refractive materials is intriguing and may offer the means of extending the phenomenon we report here to optical wavelengths. Any material that exhibits the property of negative refractive index, a property not observed in naturally occurring materials, will have a variety of practical applications, such as beam steerers, modulators, band-pass filters, and lenses permitting subwavelength point source focusing.

References and Notes

1. V. G. Veselago, *Sov. Phys. Usp.* **10**, 509 (1968).
2. J. B. Pendry, *Phys. Rev. Lett.* **85**, 3966 (2000).
3. D. R. Smith, W. J. Padilla, D. C. Vier, S. C. Nemat-Nasser, S. Schultz, *Phys. Rev. Lett.* **84**, 4184 (2000).
4. R. A. Shelby, D. R. Smith, S. C. Nemat-Nasser, S. Schultz, *Appl. Phys. Lett.* **78**, 489 (2001).
5. J. B. Pendry, A. J. Holden, D. J. Robbins, W. J. Stewart, *IEEE Trans. Microwave Theory Tech.* **47**, 2075 (1999).
6. J. B. Pendry, A. J. Holden, W. J. Stewart, I. Youngs, *Phys. Rev. Lett.* **76**, 4773 (1996).
7. D. R. Smith, N. Kroll, *Phys. Rev. Lett.* **85**, 2933 (2000).
8. R. A. Shelby, D. R. Smith, S. Schultz, data not shown.
9. L. D. Landau, E. M. Lifshitz, L. P. Pitaevskii, *Electrodynamics of Continuous Media* (Butterworth-Heinenann, Oxford, UK, ed. 2, 1984), p. 287.
10. M. Notomi, *Phys. Rev. B* **62**, 10696 (2000).
11. B. Gralak, S. Enoch, G. Tayeb, *J. Opt. Soc. Am. A* **17**, 1012 (2000).
12. We thank R. Greegor and C. Parazzoli from Boeing for helpful discussions. This research was supported by the Defense Advanced Research Projects Agency (DARPA) (contract DAAD19-00-1-0525), by DARPA through a grant from the Office of Naval Research (contract N00014-00-1-0632), and by the Air Force Office of Science Research (grant F49620-00-1-0380).

8 January 2001; accepted 22 February 2001

Three-Dimensionally Ordered Array of Air Bubbles in a Polymer Film

Mohan Srinivasarao,[1]* David Collings,[2] Alan Philips,[3]† Sanjay Patel[4]

We report the formation of a three-dimensionally ordered array of air bubbles of monodisperse pore size in a polymer film through a templating mechanism based on thermocapillary convection. Dilute solutions of a simple, coil-like polymer in a volatile solvent are cast on a glass slide in the presence of moist air flowing across the surface. Evaporative cooling and the generation of an ordered array of breath figures leads to the formation of multilayers of hexagonally packed water droplets that are preserved in the final, solid polymer film as spherical air bubbles. The dimensions of these bubbles can be controlled simply by changing the velocity of the airflow across the surface. When these three-dimensionally ordered macroporous materials have pore dimensions comparable to the wavelength of visible light, they are of interest as photonic band gaps and optical stop-bands.

A variety of templating methods that use self-assembly can create structures with submicrometer dimensions. These methods include templating using ordered arrays of colloidal particles (*1*–*5*), templating using an emulsion (*6*), honeycomb structures formed by polymers with rod-coil architecture (*7*–*10*), self-organized surfactants such as mesoporous silica (*11*–*13*), microphase-separated block copolymers (*14*–*16*), and even bacteria (*17*). Recent developments using colloidal crystal templating allow the preparation of ordered macroporous materials that have three-dimensional (3D) ordering of pores